Stopping of Light by the Dynamic Tuning of Photonic Crystal Slow Light Device

Yuji Saito[1,2] and Toshihiko Baba[1,2,*]

[1] Yokohama National University, Department of Electrical and Computer Engineering
79-5 Tokiwadai, Hodogayaku, Yokohama 240-8501, Japan
[2] CREST, Japan Science and Technology Agency
5 Sanban-cho, Chiyodaku, Tokyo 102-0075, Japan
baba@ynu.ac.jp

Abstract: We propose a simple technique of stopping light pulses using a slow-light device based on photonic crystal coupled waveguide (PCCW). Dynamically tuning the material index chirp in the PCCW adiabatically transforms slow-light pulses into stopped ones. We demonstrate this in finite-difference time-domain simulation assuming ideal and actual tuning of the index chirp. In the ideal case, the group velocity of the almost stopped pulse is reduced to 190 times smaller than that of simple slow light pulse. The smallest limit is affected by the timing error of the tuning between wavelengths. Re-ordering and stopping of a pulse train are possible by optimizing the device length and timing. As a practical tuning method, we discuss carrier effects induced by photo-excitation. Taking into account carrier distribution and free carrier absorption, the actual behaviors of stopped light are estimated. We define and evaluate an effective delay-bandwidth product, which is affected by free carrier absorption.

References and links

1. T. Baba, "Slow light in photonic crystals," Nat. Photonics **2**(8), 465–473 (2008).
2. F. Xia, L. Sekaric, and Y. Vlasov, "Ultracompact optical buffers on a silicon chip," Nat. Photonics **1**(1), 65–71 (2007).
3. M. Notomi, E. Kuramochi and T. Tanabe, "Large-scale arrays of ultrahigh-Q coupled nanocavities," Nat. Photonics **2**, 741–747 (2008).
4. F. Morichetti, A. Melloni, C. Ferrari, and M. Martinelli, "Error-free continuously-tunable delay at 10 Gbit/s in a reconfigurable on-chip delay-line," Opt. Express **16**(12), 8395–8405 (2008), http://www.opticsinfobase.org/oe/abstract.cfm?URI=oe-16-12-8395.
5. Y. A. Vlasov, M. O'Boyle, H. F. Hamann, and S. J. McNab, "Active control of slow light on a chip with photonic crystal waveguides," Nature **438**(7064), 65–69 (2005).
6. J. Li, T. P. White, L. O'Faolain, A. Gomez-Iglesias, and T. F. Krauss, "Systematic design of flat band slow light in photonic crystal waveguides," Opt. Express **16**(9), 6227–6232 (2008), http://www.opticsinfobase.org/oe/abstract.cfm?URI=oe-16-9-6227.
7. T. Baba, T. Kawaaski, H. Sasaki, J. Adachi, and D. Mori, "Large delay-bandwidth product and tuning of slow light pulse in photonic crystal coupled waveguide," Opt. Express **16**(12), 9245–9253 (2008), http://www.opticsexpress.org/abstract.cfm?URI=OPEX-16-12-9245.
8. T. Baba, J. Adachi, N. Ishikura, Y. Hamachi, H. Sasaki, T. Kawasaki, and D. Mori, "Dispersion-controlled slow light in photonic crystal waveguides," Proc. Jpn. Sci. Academy Ser. B **85**, 443–453 (2009).
9. J. Adachi, N. Ishikura, H. Sasaki, and T. Baba, "J. Adachi, N. Ishikura, H. Sasaki, and T. Baba, "Wide range tuning of slow light pulse in SOI photonic crystal coupled waveguide via folded chirping," IEEE J. Sel. Top. Quantum Electron. **16**(1), 192–199 (2010).
10. K. L. Tsakmakidis, A. D. Boardman, and O. Hess, "'Trapped rainbow' storage of light in metamaterials," Nature **450**(7168), 397–401 (2007).
11. Q. Q. Gan, Z. Fu, Y. J. Ding, and F. J. Bartoli, "Ultrawide-bandwidth slow-light system based on THz plasmonic graded metallic grating structures," Phys. Rev. Lett. **101**, 169903 (2008).
12. M. F. Yanik, and S. Fan, "Stopping light all optically," Phys. Rev. Lett. **92**(8), 083901 (2004).
13. J. Khurgin, "Adiabatically tunable optical delay lines and their performance limitations," Opt. Lett. **30**(20), 2778–2780 (2005).
14. R. S. Tucker, P.-C. Ku, and C. Chang-Hasnain, "Slow-light optical buffers – capabilities and fundamental limitations," J. Lightwave Technol. **23**, 4046–4066 (2005).

15. Y. Tanaka, J. Upham, T. Nagashima, T. Sugiya, T. Asano, and S. Noda, "Dynamic control of the Q factor in a photonic crystal nanocavity," Nat. Mater. **6**(11), 862–865 (2007).
16. Q. Xu, P. Dong, and M. Lipson, "Breaking the delay-bandwidth limit in a photonic structure," Nat. Phys. **3**, 406–410 (2007).
17. L. Yosef Mario, and M. K. Chin, "Optical buffer with higher delay-bandwidth product in a two-ring system," Opt. Express **16**(3), 1796–1807 (2008), http://www.opticsexpress.org/abstract.cfm?URI=OPEX-16-3-1796.
18. T. Tanabe, M. Notomi, H. Taniyama, and E. Kuramochi, "Dynamic release of trapped light from an ultrahigh-Q nanocavity via adiabatic frequency tuning," Phys. Rev. Lett. **102**(4), 043907 (2009).
19. D. Mori, and T. Baba, "Wideband and low dispersion slow light by chirped photonic crystal coupled waveguide," Opt. Express **13**(23), 9398–9408 (2005), http://www.opticsinfobase.org/oe/abstract.cfm?URI=oe-13-23-9398.
20. Y. Hamachi, S. Kubo, and T. Baba, "Slow light with low dispersion and nonlinear enhancement in a lattice-shifted photonic crystal waveguide," Opt. Lett. **34**(7), 1072–1074 (2009).
21. S. Adachi, *Physical properties of III–V semiconductor compounds: InP, InAs, GaAs, GaP, InGaAs, and InGaAsP* (Wiley-VCH, 1992).
22. B. R. Bennet, R. A. Soref, J. A. del Alamo, "Carrier-induced change in refractive index of InP, GaAs and InGaAsP," IEEE J. Quantum Electron. **26**, 113–122 (1990).
23. K. Nozaki, S. Kita, and T. Baba, "Room temperature continuous wave operation and controlled spontaneous emission in ultrasmall photonic crystal nanolaser," Opt. Express **15**(12), 7506–7514 (2007), http://www.opticsinfobase.org/oe/abstract.cfm?URI=oe-15-12-7506.
24. M. Aoki, H. Sano, M. Suzuki, M. Takahashi, K. Uomi and A. Takai, "Novel structure MQW electroabsorption modulator/ DFB-laser integrated device fabricated by selective area MOCVD growth," Electron. Lett. **27**, 2138–2140 (1991).

1. Introduction

The slowing and stopping of light pulses have been studied extensively for optical buffer memory and advanced time-domain signal processing in future photonic networks, interconnects, and instrumentations. Photonic nanostructures, which show large first-order dispersion $dk/d\omega$ (k: wave number, ω: angular frequency), generate on-chip *slow light* with a group velocity v_g of typically a hundred times smaller than the light velocity c in vacuum [1]. So far, coupled-resonator waveguides [2,3], all pass filters [2,4], photonic crystal (PC) waveguides [5–9], and metamaterials [10,11] have been exploited as device structures. Those except for metamaterials are made of transparent dielectric media and can be low loss devices. The delay-bandwidth product (DBP) is evaluated as an essential performance factor for these devices [1]. It indicates that large $dk/d\omega$ is obtained only in a narrow frequency bandwidth, and it constrains the maximum buffering capacity, i.e. the number of pulses buffered in the device, when the pulses are not broadened by group velocity dispersion (GVD). We have succeeded in experimentally demonstrating a high DBP of 110 in PC coupled waveguide (PCCW) of 800 μm length [8]. However, it is difficult to further enhance the DBP without increasing the length. The *stopping of light*, obtained by dynamically tuning photonic nanostructures, relaxes this constraint [12–14]. Here, $dk/d\omega$ is enhanced instantaneously by locally changing the material index of the device in the presence of light pulses. Then, the device and pulses simultaneously narrow their bandwidths, and consequently the pulses almost stop. Some studies experimentally demonstrated similar operation by controlling the *Q* factor in a single cavity or coupled cavities [15–18].

In this paper, we propose a simple dynamic tuning in chirped PCCW. In a uniform PCCW, the photonic band of a waveguide mode becomes flat at a single frequency and $dk/d\omega$ diverges to infinity, resulting in zero v_g [19]. When some structural parameters are gradually changed along the device (i.e. chirped structure), the flat band frequency is shifted so that the slow light effect is averaged over a finite bandwidth and slow light pulses can transmit with a moderate delay. The large DBP mentioned above is obtained in such a chirped PCCW. If the chirp range is changed instantaneously from an initial value to zero, slow light pulses with a wide spectrum are converted to stopped ones at a single frequency. Such dynamic tuning is possible by some practical methods. In comparison with other methods, it downsizes the device footprint because incident pulses are pre-compressed in space by the slow light effect before the tuning. Also, it allows subsequent pulses to pass through and stop in the device, which enable the re-ordering and stopping of a pulse train, respectively.

This paper first explains the principle of the tuning process in detail in Section 2. Then, the stopping of a single pulse is demonstrated in finite-difference time-domain (FDTD)

simulation in Section 3, assuming ideal tuning of material index. Here, we discuss some fundamental properties and limiting factors. In Sections 4 and 5, the re-ordering and stopping of a pulse train are demonstrated, respectively. Finally in Section 6, a real operation is discussed, assuming photo-excited carriers to change the chirp in a semiconductor device. Here, we take into account nonlinear carrier distribution, carrier plasma and band filling effects, and free carrier absorption (FCA), and discuss an effective DBP restricted by the FCA.

2. Principle

Figure 1(a) shows a schematic of the PCCW consisting of two line defects in a triangle lattice PC slab, with lattice constant a and background airhole diameter $2r$. The diameter $2r'$ of the center row of airholes and the position of other airholes are modified. Figure 1(b) shows the corresponding photonic band calculated by two-dimensional (2D) FDTD method with the periodic and absorbing boundary condition. We assume an equivalent slab index n_{eq} of 2.917, normalized hole diameters $2r/a = 0.59$, $2r'/a = 0.20$, normalized shifts $s_1/a = 0.10$ and $s_2/a = 0.20$, and a polarization parallel to the 2D plane. Two coupled modes appear, and the even mode exhibits the target flat band at a normalized frequency $\omega a/2\pi c \equiv a/\lambda = 0.257$ (λ: wavelength in vacuum). Here we define the *flat band* as that sandwiched by two white dots in Fig. 1(b), which are separated by the spectral resolution in this calculation i.e. $\Delta\omega_{res}a/2\pi c = 6.7 \times 10^{-5}$. The band shifts to higher frequencies as n_{eq} decreases along the device. When a light pulse is incident on the device, each frequency component of the pulse reaches the slow light condition of the flat band at a different position. This means that, under the slow light condition, the pulse profile is transformed into a Fourier spectral distribution. Before and after passing through this condition, it passes GVD(1) and GVD(2) in Fig. 1(b), respectively. Thus, the total GVD is compensated and the profile of the incident pulse is recovered at the output end. The bandwidth of slow light is proportional to the chirp range. On the other hand, the effective length of slow light for each frequency component is inversely proportional to the chirp range. In consequence, the delay and bandwidth are constrained by the DBP [1,14].
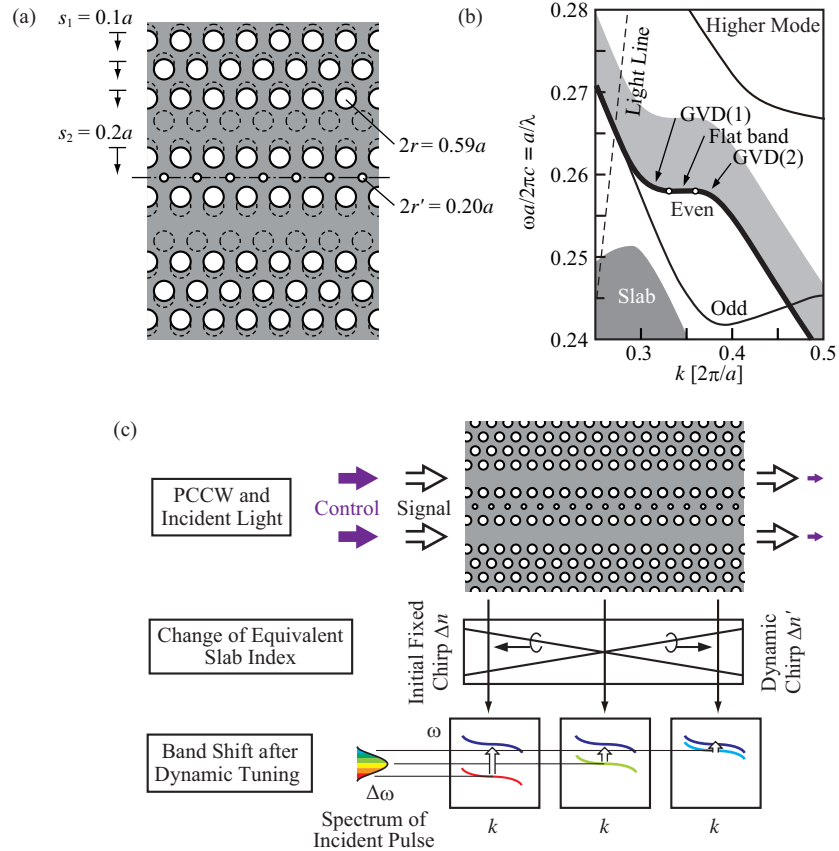
Fig. 1. Principle of stopping light pulse in chirped PCCW. (a) Structure of PCCW. Dashed lines show the original position of airholes in a triangular lattice. (b) Photonic band diagram. Thick black line shows the band of the even mode. Two white dots on this line indicate the range of flat band. Thick gray region indicate the range of shifted bands due to the initial, fixed chirp. (c) Schematic of dynamic tuning. Pump light is used to form the dynamic chirp.

Now we propose the dynamic tuning, as shown in Fig. 1(c). Here, the initial, fixed chirp is formed so that n_{eq} decreases along the device. A control pulse is incident on the device behind the signal pulse with an appropriate delay and velocity. The control pulse chases the signal pulse, and successively catches up with each frequency component that is slowing down. By means of index change induced by the pump pulse, (such as carrier effects, optical Kerr effect), n_{eq} at this position is instantaneously reduced. The amount of index change $\Delta n_{eq}'$ slopes along the device because the control pulse decays due to some propagation losses. In the ideal case, such dynamic chirp $\Delta n_{eq}'$ cancels the initial fixed chirp Δn_{eq}, and all frequency components of the situation when light at the flat-band frequency enters a chirp-less PCCW. Therefore, the delay is extended dramatically. In the reverse process, $\Delta n_{eq}'$ is removed from the input to output side, and the initial pulse profile is recovered.

3. Simulation

In this section, we demonstrate the stopping of light using 2D FDTD simulation. Here, the model in Fig. 1(a) is used, and n_{eq} decreasing linearly from 2.963 to 2.870 ($\Delta n_{eq} = 0.093$) is assumed as the initial fixed chirp for a device length $L = 125a$. This leads to a band shift of $\Delta \omega_c a / 2\pi c = 8.3 \times 10^{-3}$, depicted by the gray region in Fig. 1(b). The signal pulse is launched in the even mode, at the input end of two waveguides of the PCCW, by in-phase Gaussian excitation with $\omega_p a / 2\pi c$ centered at 0.263. Normalized time and spectral full widths at half maximum (FWHM) of the pulse are set at $c\Delta t_p / a = 290$ and $\Delta \omega_p a / 2\pi c = 1.53 \times 10^{-3}$,

respectively. This spectral FWHM is sufficiently covered by the band shift. These values correspond to $\Delta t_p = 0.39$ ps and wavelength FWHM $\Delta\lambda_p = 8.7$ nm for $a = 0.40$ μm and $\lambda_p = 1.53$ μm, which are often seen in experiments. The square control pulse forming the ideal dynamic chirp is incident with a normalized delay $c\Delta t_d/a = 720$ and a velocity of $c/3.25$, which equals the modal group velocity at $\Delta\omega a/2\pi c = 0.01$ higher than the flat band in Fig. 1(b).

Figures 2(a)-(d) compare the propagation of slow light pulse without and with the dynamic tuning. ((i)-(l) are their animations, respectively.) Without tuning (a), the pulse enters the slow light region and pauses at $ct/a = 300$, and exit at 1200. With the tuning at the best timing (c), the slow light pulse transforms into a stopped pulse, almost maintaining its profile at least until $ct/a = 3000$. We notice through careful observation that a small amount of light escapes from the stopped pulse in the forward direction. This is dues to slight timing error of the tuning between different wavelengths against the constant tuning velocity. When the tuning is early (b), the pulse propagates without pause because the tuning takes place before the light (particularly high frequency components) reaches the slow light condition. With late tuning (d), the pulse propagates with dispersion before the dispersion compensation of GVD(1) and GVD(2) is completed.

To clarify the best timing quantitatively, we estimated the motion of the pulse from the band curve. In a linearly chirped structure, the band shift with position z can be considered as the frequency shift along a fixed band [19]. Then, z and ω are related as

$$(\omega - \omega_s)/\Delta\omega_c = (z_s - z)/L \tag{1}$$

where the subscript 's' denotes the slow light condition. The time t is expressed with respect to z as

$$t(z) = \int_0^z \frac{dz}{\upsilon_g(z)} = \frac{L}{\Delta\omega_c}\left[k(\omega) - k(\omega_s + \Delta\omega_c/2)\right] \tag{2}$$

Since $k(\omega)$ is equivalent to the photonic band, we can derive the light propagation by applying Fig. 1(b) and Eq. (1) to (2). The result is shown in Fig. 2(e)-(h). Here, colors represent different frequency components overlapping with each other at the input end to form the signal pulse. Light outside of the pulse duration is neglected as they cancel with each other by interference. In (e), different frequencies branch, and the earliest and latest parts of each frequency reach the slow light condition on upper dotted and dashed lines, and exit on lower dotted and dashed lines, respectively. Finally, the different colors overlap again to form the output pulse. Thus the light propagation in (a) is well explained by (e). The gray region shows the timing window, in which all the frequency components are lying under the slow light condition. If the thick blue line indicating the motion of the tuning overlaps with the gray region, velocities of all the frequencies are fixed by the tuning. If the dynamic chirp completely cancels the initial chirp under this condition, all the frequencies are blue-shifted to the same final frequency and the velocities become almost zero. Figure 2(g) shows a case close to the ideal one, but small errors occur at edge frequencies, which are caused by the mismatch between slopes of the blue line and gray region. This is the reason that light partly escapes from the stopped pulse in (c). At off-timing (f, h), velocities fixed after the tuning are disrupted, resulting in large dispersion of the pulse.
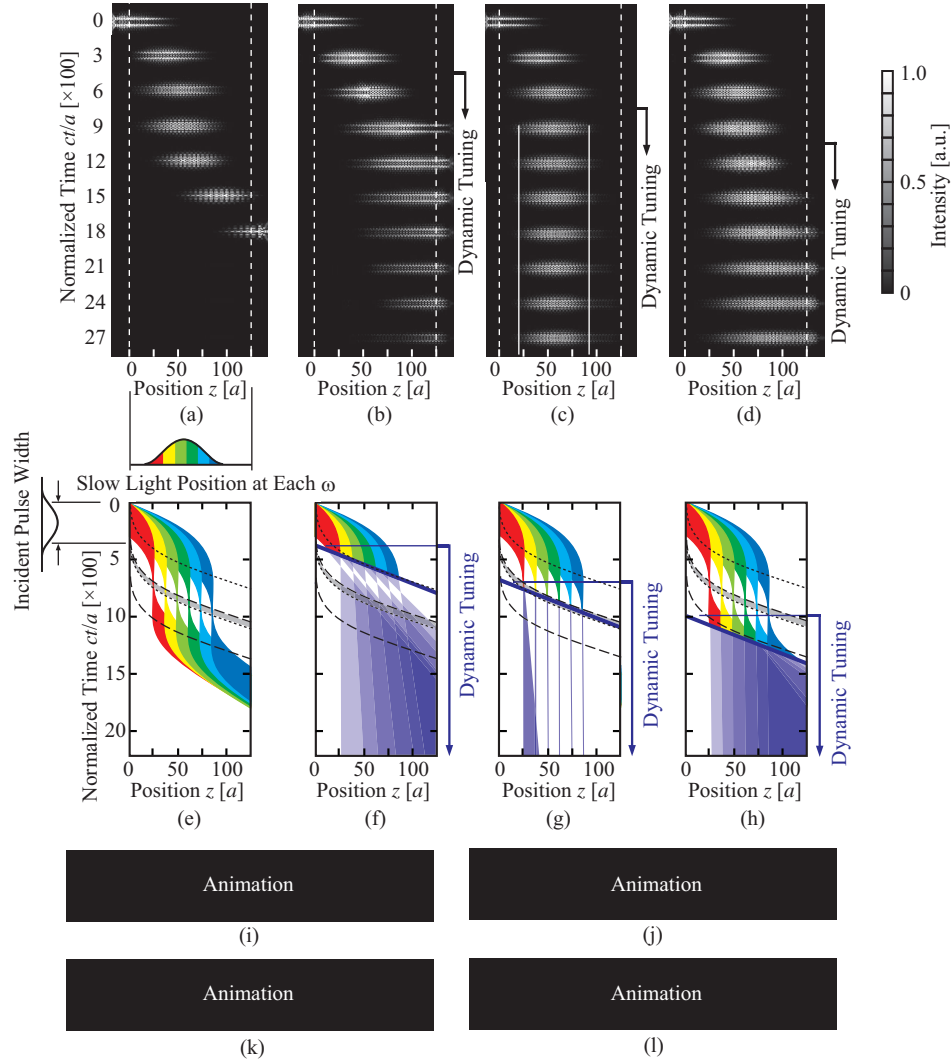
Fig. 2. FDTD simulation of dispersion-compensated slow light (a) without and (b)-(d) with dynamic tuning. Here, $c\Delta t_d/a =$ (b) 420, (c) 720, and (d) 1020. Chirped structure is lying at $z = 0 - 125a$ and n_{eq} is constant outside of this area. (e)-(h) Corresponding light propagation of each frequency component estimated from photonic band in Fig. 1(b). Colors indicate different frequencies. Gray region indicates the slow light condition. (i)-(l) Animations corresponding to (a)-(d), respectively. (Media 1) (Media 2) (Media 3) (Media 4)

From (2), the delay due to slow light, Δt_s, is given as

$$\Delta t_s = (L / \omega_c)\Delta k \tag{3}$$

where Δk_s is the shift of k at the flat band (distance between white dots in Fig. 1(b)). To achieve the stopping of light, the gray region must be opened by the condition $\Delta t_s - \Delta t_p > 0$. For a Gaussian pulse satisfying $\Delta t_p(\Delta \omega_p/2\pi) = 0.44$, this condition is rewritten as

$$(\Delta \omega_p / \Delta \omega_c)(\Delta k_s / 2\pi)L > 0.44 \tag{4}$$

From Fig. 1(b) and parameters assumed above, $\Delta \omega_p/\Delta \omega_c = 0.18$, $\Delta k_s/2\pi = 0.028/a$ and $L = 125a$, which lead to $(\Delta \omega_p/\Delta \omega_c)(\Delta k_s/2\pi)L = 0.63 > 0.44$. Here, the spectral efficiency $\Delta \omega_p/\Delta \omega_c$ will be enhanced up to 0.5 by narrowing the signal pulse and/or the chirp range. Δk_s increases

slightly when the structure is optimized; the maximum $\Delta k_s/2\pi$ would be limited to around $0.04/a$ [19]. Then, the shortest L satisfying (4) is derived as $22a$, which is 9 μm for $a = 0.40$ μm.

Figure 3 summarizes velocities at three different parts of the pulse. White circles show the velocity at the weighted center, which is equivalent to v_g. Blue and red circles show those at front and back ends whose intensity is 10% of the pulse peak. Dispersion can be evaluated from their difference. For example, dispersion is minimum and $v_g = 4.2 \times 10^{-4}c$ (group index $n_g \equiv c/v_g = 2400$) at $c\Delta t_d/a = 720$ when the pulse looks to be almost stopped in Fig. 2(c). From this value, the normalized DBP, defined as $n_g(\Delta\omega_p/\omega_p)$ [1], is evaluated to be 14. For slow light without tuning, it is evaluated from the delay inside the device in Fig. 2(a) and the spectral FWHM $\Delta\omega_p$ to be 0.075. Thus, the tuning provides 190-fold enhancement. Since the spectral FWHM $\Delta\omega_p$ is 5.4 times narrower than the slow light band $\Delta\omega_c$ in this simulation, the normalized DBP without tuning can be enhanced by expanding $\Delta\omega_p$ and/or narrowing $\Delta\omega_c$. The spectra should be optimized similarly for the stopped pulse to maintain its advantage. However, if $\Delta\omega_p$ is comparable to $\Delta\omega_c$, the timing error at low frequencies increases and the stopped pulse is dispersed more severely. If the tuning velocity is not constant but changes along the device so that the blue line in Fig. 2(e)-(h) is always included inside the gray region, the error will be neglected and v_g will be minimized closer to zero.
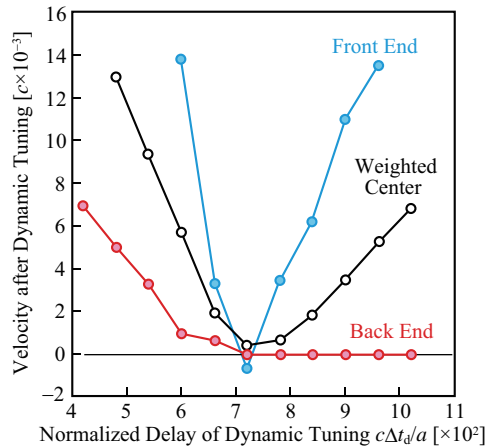

Fig. 3. Velocities at three different parts of slow light pulse after dynamic tuning, which is calculated with normalized delay of the tuning against signal light.

4. Re-ordering of pulses

If the dynamic tuning is performed with cavities, the transmission is limited inside the resonant spectrum. Therefore, when multiple pulses with the same spectrum are incident on the device, subsequent pulses cannot pass through the device after an earlier pulse is stopped by the tuning. In contrast, our method maintains continuous pass-bands around the frequency of stopped light, and so subsequent pulses can pass while earlier pulses are stopped. The order of pulses can be changed by releasing the earlier pulse after the subsequent pulses pass by, as demonstrated in Fig. 4. Here, four Gaussian pulses of $c\Delta t_p/a = 290$ are successively launched with a peak-to-peak interval of $c\Delta t_i/a = 960$. The tuning is performed for the second pulse with $c\Delta t_d/a = 720$ and a duration equal to the interval. (b) shows a complicated light intensity profile due to overlap of pulses, but the corresponding animation (d) displays counterchange of the second and third pulses. The third pulse incident during the tuning propagates with a constant v_g. As observed in (c), the slow light pulses (first, last), the stopped pulse (second), and the non-stop pulse (third) almost maintain their initial shape at the output end. Such pulse re-ordering will be meaningful for some signal processing if each pulse has its own intensity, phase, quantum information, etc.
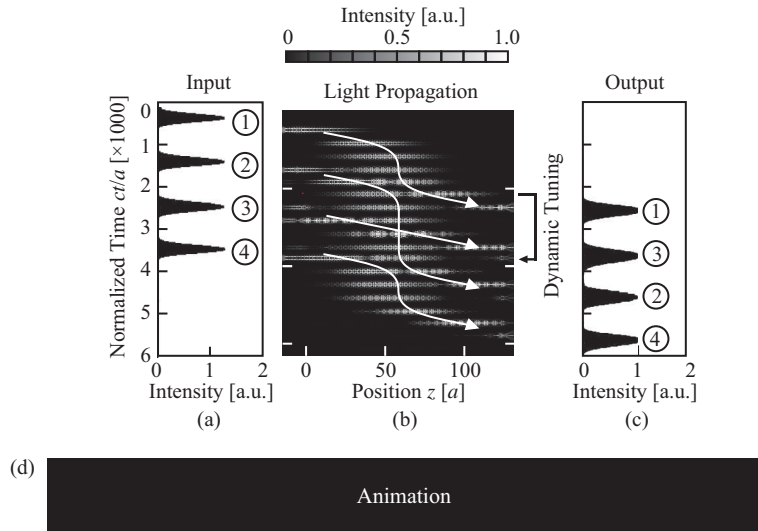
Fig. 4. Re-ordering of pulses demonstrated in FDTD simulation. (a) Profile of input pulses. (b) Time evolution of pulse intensity distribution. (c) Profile of output pulses. (d) (Media 5) Animation corresponding to (b).

5. Stopping of pulse train

For optical buffering, it is particularly important to stop an entire pulse train simultaneously. When cavities are used for stopping pulses, it requires many cavities each assigned to one pulse, and complicated tuning process. Here, we show two different approaches to achieve this using our simple tuning process.

As noted in Section 2, the pulse incident on chirped PCCW is expanded into a Fourier spectral distribution due to GVD(1). When a pulse train is incident, pulses do not pause separately but their spectral distributions overlap and slow down, keeping their initial time differences. If timing of the tuning is optimized for one pulse, the timing error occurs for other pulses, resulting in severe dispersion. The key is the blue line of the tuning overlapping with the gray region $\Delta t_s - \Delta t_p$. In Fig. 2(e)-(h), the gray region is opened for the FWHM of one pulse. For densely-packed return-to-zero pattern of M pulses, Δt_p is extended to $(2M-1)\Delta t_p$. Therefore, Δt_s must be extended similarly to keep the gray region still opening. Such a situation is obtainable by elongating the device $(2M-1)$ times without changing the chirp range Δn_{eq}, so that the pulses decelerate and accelerate more slowly. For example, let us consider two pulses and a three-fold longer device, i.e. $L = 375a$. The second pulse is incident with an interval of $c\Delta t_i/a = 720$. Then, the optimum delay of the tuning becomes $c\Delta t_d/a = 2520$. Figure 5 shows the FDTD simulation of stopping two pulses. Incident pulses overlap and exhibit a complex interference pattern under the slow light condition, which is almost fixed and stopped after the tuning. It goes into action but does not separate into two pulses again after the tuning is removed. This is due to the incomplete dispersion compensation of the first structure. When the interval is slightly extended to $c\Delta t_i/a = 720$, clear separation was confirmed in the same simulation. In Section 3, we discussed the shortest length of the device required for stopping one pulse with ideal parameters to be $22a$. Therefore, M ($\gg 1$) pulses can be buffered in the device of approximately $44aM$ length, e.g. 1.8 mm with $a = 0.4$ μm for 100 pulses if the incomplete dispersion compensation is improved.
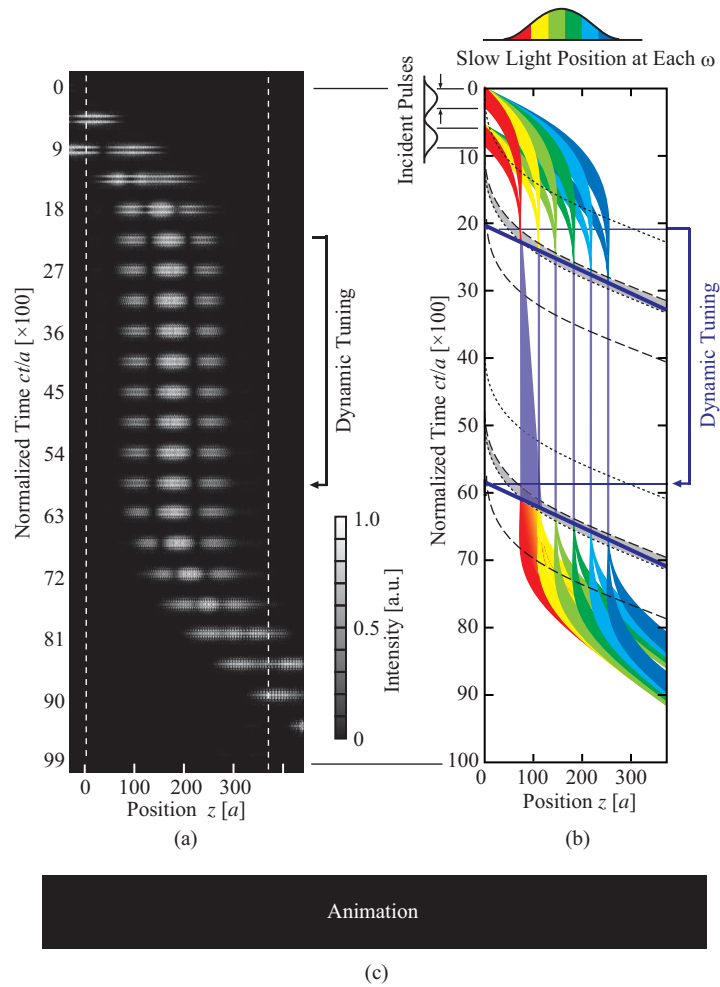
Fig. 5. FDTD simulation of stopping two pulses in three-fold longer PCCW. (a) Light intensity profile. (b) Light propagation of each frequency component estimated from photonic band. (c) (Media 6) Animation corresponding to (a).

The other method for stopping a pulse train is to divide areas, each of which stop one pulse. Figure 6 shows the case of stopping two pulses in a double-step chirped structure. Here, two chirped PCCWs are simply connected in series. Without tuning, pulses repeat slowing and moving in the PCCWs. If a moderate interval is set between the pulses, they slow simultaneously. If the tuning is performed at this moment, the pulses are equally stopped. Ideally, the tuning should cancel Δn_{eq} in each PCCW. But it is difficult to form a multi-step dynamic chirp. Here we use the single-step dynamic chirp with twice larger $\Delta n_{eq}'$, i.e. 0.186. Then, the index slope of each chirp is flattened although their indices after the tuning are not the same. In the FDTD simulation, delays of the second pulse and tuning are set to be $c\Delta t_d/a = 1440$ and 2580, respectively. Figure 7(a) shows the light propagation in a two-step chirped structure with $\Delta n_{eq} = 0.093$. The tuning at the first chirping does not operate as expected; strong reflection occurs at the boundary with the index discontinuity. To confirm the expected operation, the same simulation was performed for a smaller Δn_{eq} of 0.0093, as shown in Fig. 7(b). Here, two pulses stop simultaneously although weak reflection still remains. After removing $\Delta n_{eq}'$, the two pulses appear at the output end. This approach can be applied to M pulses using M-step chirp. Two drawbacks are the reflection at the boundary particularly for pulses with a short interval and N-fold $\Delta n_{eq}'$ required.
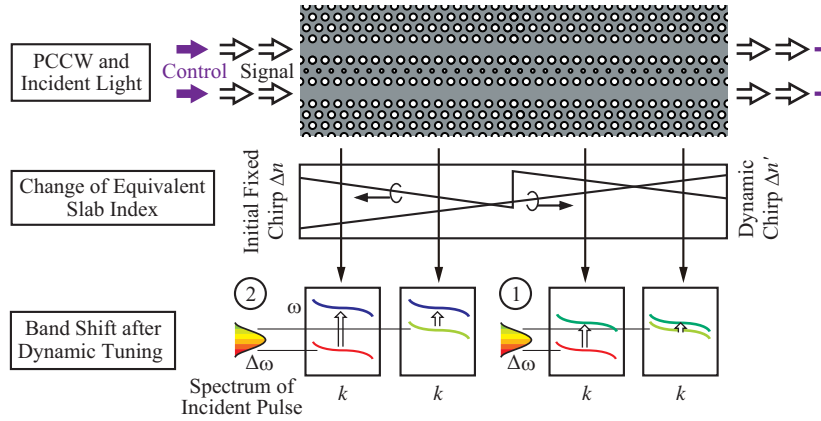
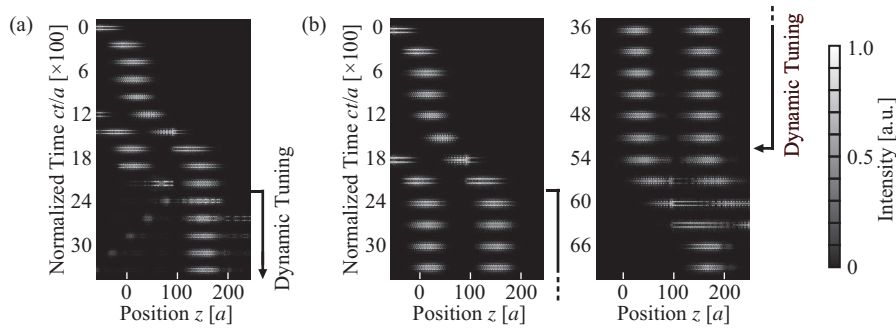Fig. 6. Schematic of dynamic tuning against two pulses in a two-step chirped structure

Fig. 7. FDTD simulation of stopped two pulses in two-step chirped PCCW. (a) Light intensity profile for $\Delta n_{eq} = 0.093$ and (b) 0.0093.

6. Practical dynamic tuning using photo-excited carriers

So far, we presented the dynamic tuning with an ideal index change. To realize such index change, let us discuss carrier effects induced by photo-excitation, i.e. carrier plasma dispersion and band filling effects. As discussed in Section 2, pump light is incident on the device in the same manner as signal pulse. We can consider linear inter-band absorption and nonlinear two-photon absorption [20] of pump light at frequencies higher and lower than the bandgap frequency of the slab material, respectively. Let us discuss the linear absorption as it generates a carrier slope closer to a linear one, which is suitable for canceling the initial linear chirp. It should be noted that FCA cannot be neglected to estimate the real propagation of signal pulse in this approach.

The totally absorbed power in a distance from 0 to z, $P_{ab}(z)$, is given by

$$P_{ab}(z) = P_{ex}(1 - e^{-\Gamma \alpha_{ab} z}) \tag{5}$$

where P_{ex} is the pump power launched on the device, and Γ and α_{ab} are the optical confinement factor and absorption coefficient of pump light in the slab, respectively. The carrier density distribution $N(z)$ is then

$$N(z) = \frac{\tau_c dP_{ab}(z)/dz}{\hbar \omega_{ex} S} \tag{6}$$

where τ_c is the carrier lifetime, and ω_{ex} and S are the angular frequency and modal cross-section of pump light. The change of material index due to carrier plasma dispersion, Δn_{CPD}, is

not sensitive to the signal pulse frequency ω_p. According to the Drude's model, Δn_{CPD} and FCA coefficient α_{FCA} are

$$\Delta n_{CPD}(z) = -\frac{e^2 N(z)}{2n\varepsilon_0 \omega_p^2}\left(\frac{1}{m_e^*} + \frac{1}{m_h^*}\right) \quad , \quad \alpha_{FCA}(z) = \frac{e^3 N(z)}{n\varepsilon_0 c\omega_p^2}\left(\frac{1}{\mu_e m_e^{*2}} + \frac{1}{\mu_h m_h^{*2}}\right) \quad (7)$$

where e is the electron charge, n is the initial index of the slab without free carriers, ε_0 is the dielectric constant in vacuum, m_e^* and m_h^* are the effective masses of electron and hole, and μ_e and μ_h are their mobilities, respectively. On the other hand, the band filling effect is sensitive to ω_p. When ω_p is close to bandgap frequency of the slab material, it becomes larger than Δn_{CPD}, as has been studied for GaInAsP semiconductors. Since it depends on N almost linearly, we roughly express the total index change Δn as $\gamma\Delta n_{CPD}$, where γ denotes the enhancement by the band filling effect. The dynamic chirp $\Delta n_{eq}'$ is then expressed as

$$\Delta n_{eq}'(z) \equiv n_{eq}\left[\Gamma\frac{n+\Delta n(z)}{n} + (1-\Gamma)\right] - n_{eq} = \Gamma\Delta n(z)n_{eq}/n$$

$$= -\gamma\frac{e^2\tau_c n_{eq}\Gamma^2\alpha_{ex}e^{-\Gamma\alpha_{ex}z}P_{ex}}{2n^2\varepsilon_0\hbar\omega_{ex}\omega_p^2 S}\left(\frac{1}{m_e^*} + \frac{1}{m_h^*}\right) \quad (8)$$

The equivalent FCA coefficient $\alpha_{eq}(z)$ is

$$\alpha_{eq}(z) = \Gamma\alpha_{FCA}(z) = \frac{e^3\tau_c\Gamma^2\alpha_{ex}e^{-\Gamma\alpha_{ex}z}P_{ex}}{n\varepsilon_0 c\hbar\omega_{ab}\omega_p^2 S}\left(\frac{1}{\mu_e m_e^{*2}} + \frac{1}{\mu_h m_h^{*2}}\right) \quad (9)$$

Now, let us consider a GaInAsP PC slab with $m_e^* = 0.045m_0$, $m_h^* = 0.47m_0$, $\mu_e = 1100$ cm^2/Vs, $\mu_h = 70$ cm^2/Vs [21,22], $\tau_c = 100$ ps [23], $\gamma = 3$ [22], $n = 3.45$, $\Gamma = 0.89$, $S = 0.3$ µm^2 (typical values for GaInAsP and PCCW at $\lambda \sim 1.55$ µm), $\Delta n_{eq} = 0.0093$, $a = 0.4$ µm and $L = 500$ µm ($= 1250a$). We can consider α_{ex} and P_{ex} as externally controllable parameters; α_{ex} can be controlled by changing the composition of GaInAsP and/or pump frequency near the bandgap. These parameters are chosen so that the dynamic chirp cancels the initial chirp, i.e. $\Delta n_{eq}'(0) - \Delta n_{eq}'(L) = 0.0093$. We ignored the scattering loss caused by the disordering in actual devices to investigate the influence of FCA. Fig. 8 shows the calculated distributions of $N(z)$, $\Delta n_{eq}'(z)$ and $\alpha_{eq}(z)$. When α_{ex} is small, a high P_{ex} is needed to generate the above difference in $\Delta n_{eq}'$, while a linear distribution is easily formed. But in this case, the carrier density becomes higher, resulting in large FCA. When α_{ex} is large, a small P_{ex} is sufficient to obtain the difference, and so the FCA is small. However, the distribution becomes nonlinear.
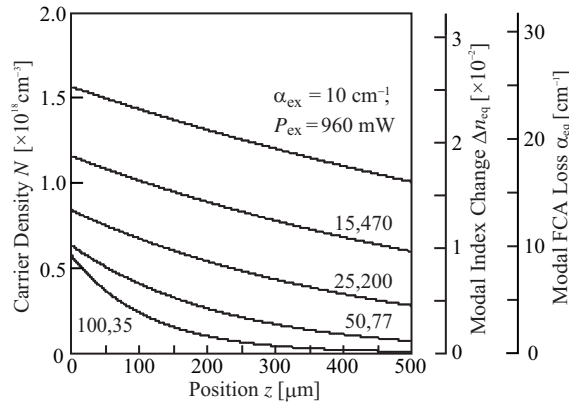

Fig. 8. Distributions of photo-excited carrier density, index change by carrier effects, and FCA.
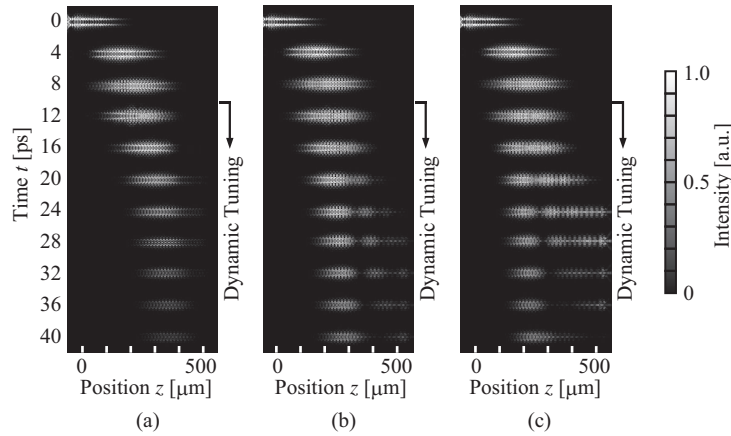
Fig. 9. FDTD simulation of stopped pulse assuming photo-excited carriers in GaInAsP PCCW. (a) α_{ex} = 25, (b) 50, and (c) 100 cm^{-1}.

The FDTD simulation is performed, assuming Δt_p = 3.9 ps and λ_p = 1.521 μm. For the long device of L = 500 μm, however, a long computation time is necessary even in 2D. To reduce this load, actual calculation is done by scaling L and t to 1/10 times and α_{ex}, α_{eq}, Δn_{eq}, and $\Delta n_{eq}'$ to 10 times. The results are summarized after scaling back, as shown in Fig. 9. At α_{ex} = 50 cm^{-1}, the pulse stops without dispersion because almost linear distribution in $\Delta n_{eq}'$ is formed. However, the pulse severely decays due to the large FCA; the photon lifetime τ_{ph} after the tuning is as short as 36 ps. At α_{ex} = 100 cm^{-1}, the pulse dispersed due to nonlinear distribution while propagation extends due to the small FCA. A solution for suppressing both dispersion and FCA is to modify α_{ex} with z so that a linear distribution is formed even for minimal carrier excitation. Such α_{ex} is obtainable when using the selective-area growth of GaInAsP in metal-organic vapor-phase epitaxy [24]; a sloped bandgap frequency is formed by shaping the growth mask. If dispersion disappear for α_{ex} = 50 cm^{-1}, τ_{ph} will double. To extend τ_{ph} drastically, the initial chirp Δn_{eq} must be much smaller than the assumed value. As noted in Section 2, Δn_{eq} determines the slow light band before the tuning; Δn_{eq} = 9.3 × 10^{-3} corresponds to a bandwidth of 760 GHz for the assumed parameters. If a narrower bandwidth such as 76 GHz is sufficient for one's purpose, Δn_{eq} can be reduced to 9.3 × 10^{-4}. In proportion to this, the FCA is suppressed and τ_{ph} will extend by 10 times. This discussion suggests that the product between the bandwidth limited by Δn_{eq} and the photon lifetime limited by the FCA can be defined as an effective DBP for stopping light using carrier effects. It is calculated to be 27 for the above values. Let us consider a situation that some amount of loss in the device can be compensated by integrated or external amplifiers. These days, standard erbium-doped optical fiber amplifiers used for pre-amplification provide a 25 dB gain. If a −25 dB decay of stopped light is recoverable by such amplification, τ_{ph} extends to 0.2 ns and the effective DBP will be 152. In the case without tuning, the maximum DBP in experiments is 110 for 800-μm long PCCW, suggesting that it will be 69 for 500-μm long device from the linear dependence on L. Therefore, the effective DBP for stopping light can be larger than simple slow light if such decay is acceptable.

7. Conclusion

We proposed and theoretically demonstrated a method of stopping slow light pulse by dynamically cancelling the index chirp in photonic crystal coupled waveguide. In the FDTD simulation, the group velocity of subpicosecond optical pulse is drastically reduced to at least 190 times lower than that of simple slow light when the tuning is performed with the best timing. The complete stopping will be possible by optimizing the velocity of the pump pulse. It was also shown that this method allows the stopping of two continuous pulses by elongating the device to three times. This discussion can be extended to stopping M pulses in $(2M-1)$

times longer device. Therefore, it has a potential of buffering arbitrary optical signals. Finally, carrier plasma and band filling effects induced by photo-excited carriers were considered for real tuning. The stopping of light is observed for real parameters of GaInAsP device. Here, the nonlinear distribution of carriers and free carrier absorption enhance the dispersion and loss, respectively. From their exclusive relation, the effective delay-bandwidth product was defined and estimated to be 27 (or 152 if a recoverable loss is acceptable). This value is comparable or slightly larger than that of simple slow light. To improve this value essentially, investigation of some other tuning mechanisms such as nonlinear optical Kerr effect and electro-optic effect, which do not use carrier excitation, will be necessary.